Supporting Information

Beyond the "Spine of Hydration": Chiral SFG Spectroscopy Detects DNA First Hydration Shell and Base Pair Structures

Ethan A. Perets[1#†], Daniel Konstantinovsky[1,2§†], Ty Santiago[1], Pablo E. Videla[1ᴺ], Matthew Tremblay[1], Luis Velarde[3], Victor S. Batista[1], Sharon Hammes-Schiffer[1,4]*, E. C. Y. Yan[1]*

[1]Department of Chemistry, Yale University, New Haven, CT 06520, USA

[2]Department of Molecular Biophysics and Biochemistry, Yale University, New Haven, CT 06520, USA

[3]Department of Chemistry, University at Buffalo, State University of New York, Buffalo, NY 14260, USA

[4]Department of Chemistry, Princeton University, Princeton, NJ 08544, USA

[#]Current Address: Department of Molecular Biology, University of Texas Southwestern Medical Center, Dallas, TX 75390, USA

[§]Current Address: Department of Chemistry, Columbia University, New York, NY 10027, USA

[ᴺ]Current Address: Schrödinger, LLC, New York, NY 10036, USA

[†]Equal Contribution

*Corresponding Authors

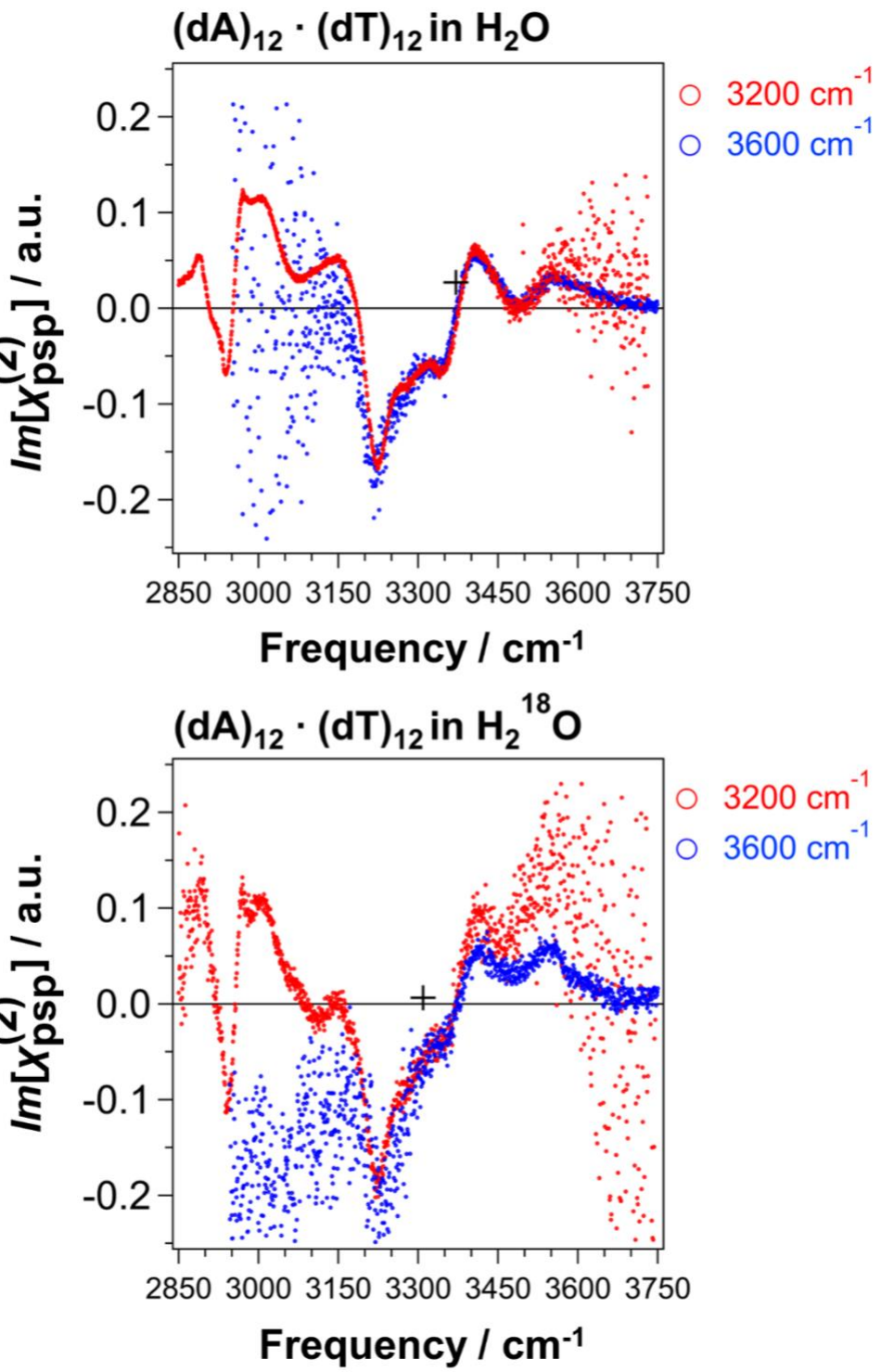

Figure S1. Spectra of $(dA)_{12} \cdot (dT)_{12}$ dsDNA prepared in H_2O (top) and in $H_2{}^{18}O$ (bottom) measured in the C-H/N-H/O-H region with the *psp* polarization. Spectra were recorded in two windows with the broad bandwidth infrared beam at frequencies centered at 3200 cm^{-1} (red) and 3600 cm^{-1} (blue). Spectra from each window were stitched to produce the spectra in Figure 2 of the main text.

Parameter	Value $(dA)_{12} \cdot (dT)_{12}$ (H_2O) Figure 2	Value $(dA)_{12} \cdot (dT)_{12}$ ($H_2{}^{18}O$) Figure 2	Assignments
A_1	-3.7 ± 0.2	-4.6 ± 0.2	OH (water)
ω_1	3503.2 ± 2.1	3465.7 ± 1.9	
$\Delta\nu_1$	150.0		
Γ_1	80.8 ± 2.7		
A_2	9.2 ± 0.5	6.8 ± 0.3	NH_aH_b (adenine)
ω_2	3401.3 ± 1.5		
Γ_2	55.5 ± 1.7		
A_3	-2.5 ± 0.3	-0.6 ± 0.2	NH_aH_b (adenine)
ω_3	3356.9 ± 0.8		
Γ_3	25.1 ± 1.8		
A_4	15.9 ± 1.1	8.5 ± 0.6	OH (water)
ω_4	3222.5 ± 2.4	3215.0 ± 3.7	
$\Delta\nu_4$	79.2		
Γ_4	95.1 ± 3.0		
A_5	-4.9 ± 0.3	-4.0 ± 0.2	NH_aH_b (adenine)
ω_5	3219.7 ± 0.2		
Γ_5	24.2 ± 0.6		
A_6	18.9 ± 0.6	22.4 ± 1.0	CH (DNA)
ω_6	2998.3 ± 1.0		
Γ_6	55.7 ± 1.0		
A_7	2.4 ± 0.3	2.8 ± 0.3	CH (DNA)
ω_7	2966.4 ± 0.2		
Γ_7	15.0 ± 0.8		

Table S1. Fitting parameters for $(dA)_{12} \cdot (dT)_{12}$ dsDNA prepared in H_2O and in $H_2{}^{18}O$ (Figure 2) according to equation 2 (see Methods in main text).

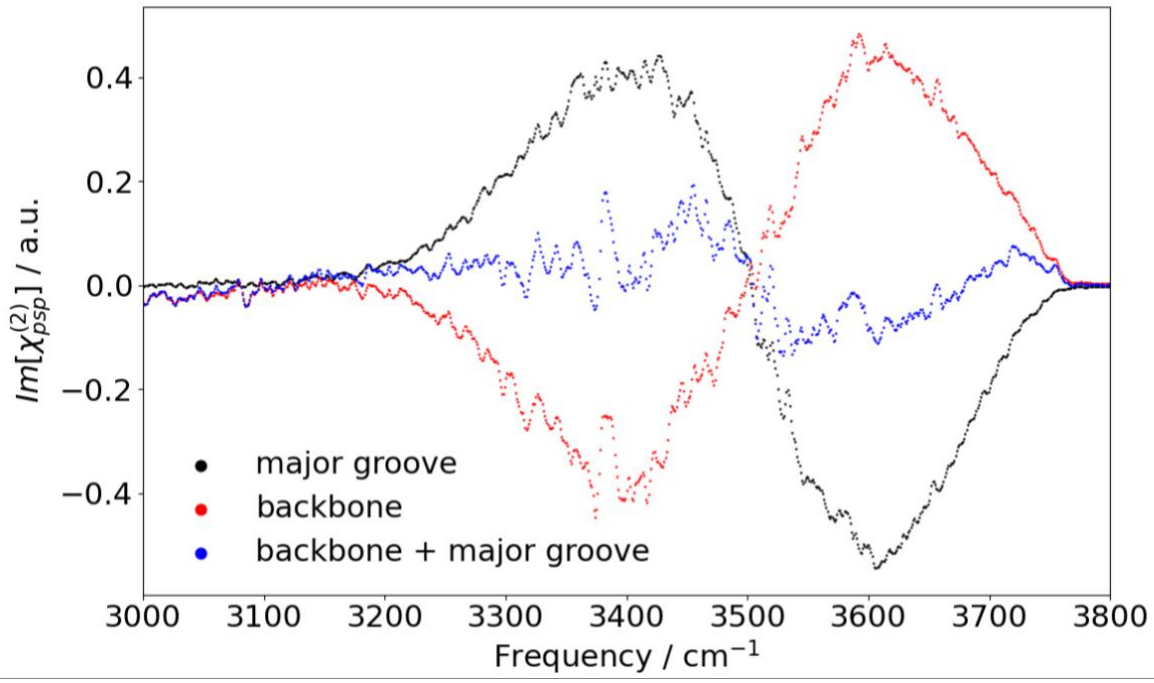

Figure S2. Calculation of the chiral SFG response of water molecules hydrating the major groove and backbone of $(dA)_{12} \cdot (dT)_{12}$ dsDNA. The chiral SFG signals from the major groove (black) and backbone (red) have opposite phase and nearly completely cancel (blue).

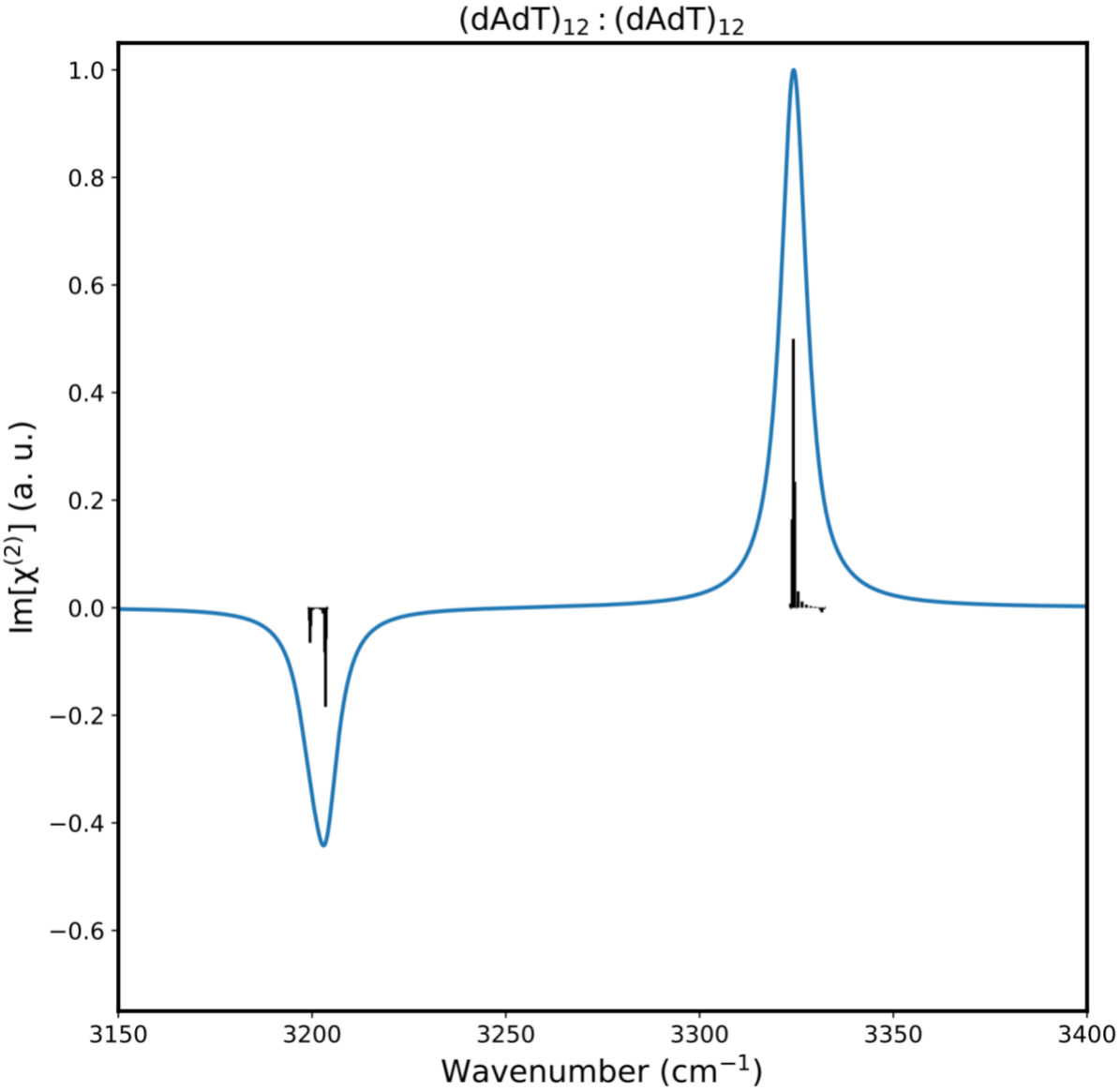

Figure S3. Gas-phase calculation of the phase-resolved chiral SFG response of $(dAdT)_{12} \cdot (dTdA)_{12}$ dsDNA in the N-H/O-H stretching region. Histogram lines (black) show vibrational intensity and phase. The spectral frequencies were scaled by a factor of 0.95. The data shown is for values of the Euler angles $\theta = 0°$ and averaged around ψ and φ. These parameters recapitulate the experimental setup described by Petersen and co-workers.[1]

Supplementary Description of Density Functional Theory and Exciton Model Calculations

Normal modes of AT base pair

In **Figure S4** we present the AT Watson-Crick base pair model used to obtain vibrational information in the NH stretching region. This model includes an explicit water molecule bound to the NH_2 group on the adenine to partially account for the solvation of this group.[2, 3] Normal mode displacement vectors and unscaled harmonic frequencies for the three relevant NH stretching modes computed at the ωB97XD/cc-pvdz level of theory[4, 5] are shown in **Figure S5**. The mode at 2962 cm^{-1} corresponds to a localized vibration of the $N-H\cdots N$ motif. Interestingly, this mode shows a big redshift for the typical NH stretching region, presumably due to the strong intermolecular hydrogen-bond interaction between the base pairs. Note that strong, red-shifted vibrations are typically associated with anharmonic vibrations and are not well described at the harmonic level; therefore, we did not include this mode in the exciton description. The modes at 3370 cm^{-1} and 3503 cm^{-1} correspond to symmetric and asymmetric NH stretching of the NH_2 group, respectively, and were employed in the exciton model to compute the SFG response of the $(dA)_{12}\cdot(dT)_{12}$ dsDNA. In **Table S2** we summarize the transition dipoles and transition Raman polarizability tensors for these modes (computed under the harmonic approximation).

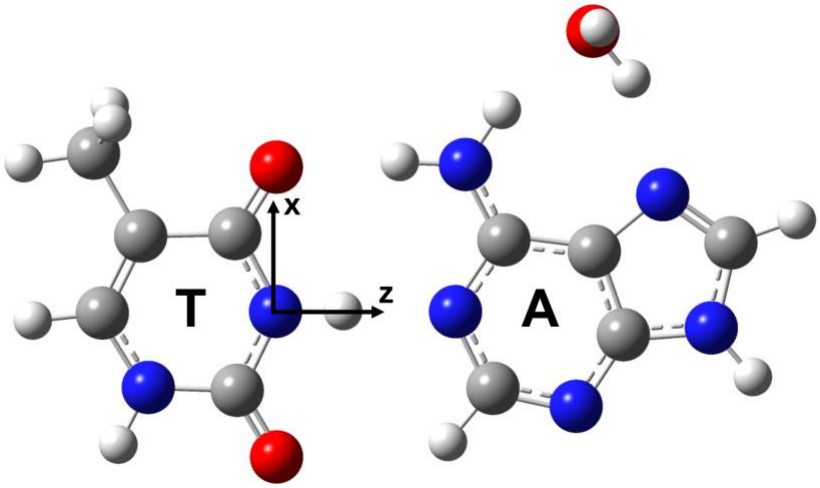

Figure S4. Solvated AT base pair used to model the NH stretching region. Also shown is the molecular axis used to define the transition dipole and transition polarizability tensors shown in **Table S2**.

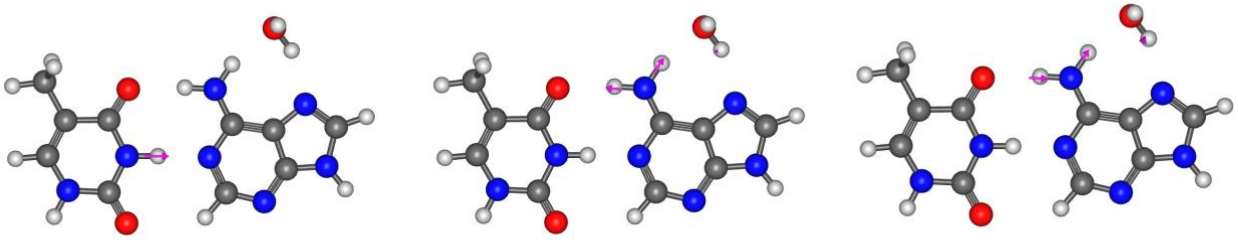

Figure S5. NH stretching normal mode displacement vectors and unscaled harmonic frequencies for the NH stretching modes.

		Sym. NH	Asym. NH
Frequency (cm^{-1})	ω	3370	3503
Transition Dipole ($e.a_0$)	μ_x	0.064	-0.023
	μ_y	0.002	0.001
	μ_z	-0.061	-0.135
Transition Polarizability (a_0^3)	α_{xx}	1.321	-0.966
	α_{xy}	0.069	-0.089
	α_{xz}	0.173	-0.248
	α_{yy}	0.046	-0.057
	α_{yz}	0.027	-0.011
	α_{zz}	1.704	1.441

Table S2. Computed vibrational parameters for the NH stretching modes of AT base pairs. Transition dipole and polarizability are computed under the harmonic approximation as $\mu_i = \sqrt{\frac{\hbar}{2\omega_q}}\frac{\partial \mu_i}{\partial Q_q}$ and $\alpha_{ij} = \sqrt{\frac{\hbar}{2\omega_q}}\frac{\partial \alpha_{ij}}{\partial Q_q}$, where α_{ij} and μ_i are elements of the polarizability and dipole moment, respectively, in the molecular frame (see **Figure S4**), and Q_q is the normal coordinate of the q-th vibrational mode with frequency ω_q.

Exciton model parametrization

To simulate the SFG spectra of the double-strand $(dA)_{12} \cdot (dT)_{12}$, an exciton model was parametrized on a $(A)_3 \cdot (T)_3$ model using the Hessian matrix reconstruction (HMR) method,[6-8] briefly described below. To this end, we consider a triple-layer ($N_{bp} = 3$) structure of stacked (geometry-optimized) AT base pairs, each base-pair containing $N_{at} = 33$ atoms, consistent with the average values of an ideal B-DNA, with distances and relative orientations (twist angle) between the layers of 3.4 Å and 36°, respectively (see **Figure S6**). A frequency analysis was performed on this model to obtain the full mass-weighted $3N_{bp}N_{at} \times 3N_{bp}N_{at}$ Hessian matrix F, which can be written as

$$F = \begin{pmatrix} F^{(1)} & \cdots & \cdots \\ \cdots & F^{(2)} & \cdots \\ \cdots & \cdots & F^{(3)} \end{pmatrix} \quad \text{(S1)}$$

where $F^{(j)}$ is the $3N_{at} \times 3N_{at}$ block matrix for the *j*-th base pair that contains the second derivatives of the energy with respect to the atomic coordinates of the *j*-th base pair. Each $F^{(j)}$ block was subsequently diagonalized to obtain localized eigenvectors $u_k^{(j)}$ and eigenvalues $\lambda_k^{(j)}$ corresponding to localized vibrational modes in each base pair. Of all the $3N_{at}$ vibrational modes, we focus on the two corresponding to the symmetric and asymmetric N–H stretch normal modes, whose eigenvectors are hereafter labeled $u_s^{(j)}$ and $u_a^{(j)}$, respectively. The corresponding two eigenvectors are used to construct a $3N_{at} \times 2N_{bp}$ matrix U, of the form:

$$U = \begin{pmatrix} u_s^{(1)} & u_a^{(1)} & 0 & 0 & 0 & 0 \\ 0 & 0 & u_s^{(2)} & u_a^{(2)} & 0 & 0 \\ 0 & 0 & 0 & 0 & u_s^{(3)} & u_a^{(3)} \end{pmatrix} \tag{S2}$$

which is used to transform the original mass-weighted Hessian matrix F into the reconstructed Hessian matrix in the local basis modes, F_{HMR}:

$$F_{HMR} \equiv U^T F U = \begin{pmatrix} \lambda_s^{(1)} & 0 & F_{ss}^{(1,2)} & F_{sa}^{(1,2)} & F_{ss}^{(1,3)} & F_{sa}^{(1,3)} \\ 0 & \lambda_a^{(1)} & F_{as}^{(1,2)} & F_{aa}^{(1,2)} & F_{as}^{(1,3)} & F_{aa}^{(1,3)} \\ F_{ss}^{(2,1)} & F_{sa}^{(2,1)} & \lambda_s^{(2)} & 0 & F_{ss}^{(2,3)} & F_{sa}^{(2,3)} \\ F_{as}^{(2,1)} & F_{aa}^{(2,1)} & 0 & \lambda_a^{(2)} & F_{as}^{(2,3)} & F_{aa}^{(2,3)} \\ F_{ss}^{(3,1)} & F_{sa}^{(3,1)} & F_{ss}^{(3,2)} & F_{sa}^{(3,2)} & \lambda_s^{(3)} & 0 \\ F_{as}^{(3,1)} & F_{aa}^{(3,1)} & F_{sa}^{(3,2)} & F_{aa}^{(3,2)} & 0 & \lambda_a^{(3)} \end{pmatrix} \tag{S3}$$

The reconstructed Hessian matrix F_{HMR} includes the force constants of the symmetric and asymmetric N–H stretch modes localized in each base pair as the diagonal elements (i.e., $\lambda_k^{(j)} = \left(\omega_k^{(j)}\right)^2$) as well as off-diagonal elements representing the inter-strand "force constant" couplings between different base pairs. The exciton Hamiltonian matrix H is obtained from the HMR Hessian matrix by normalizing each element in F_{HMR} as $(F)_{ij} = \frac{(F)_{ij}}{\sqrt{(F)_{ii}(F)_{jj}}}$ (to transform from force constants to frequencies) and averaging over equivalent site interactions (e.g., $F_{ss}^{(1,2)}$ and $F_{ss}^{(2,3)}$ represent first-neighbor interactions between symmetric NH stretches), resulting in:

$$H/\hbar = \begin{pmatrix} \omega_s & 0 & J_{ss}^{(1)} & J_{as}^{(1)} & J_{ss}^{(2)} & J_{as}^{(2)} \\ 0 & \omega_a & J_{as}^{(1)} & J_{aa}^{(1)} & J_{as}^{(2)} & J_{aa}^{(2)} \\ J_{ss}^{(1)} & J_{as}^{(1)} & \omega_s & 0 & J_{ss}^{(1)} & J_{as}^{(1)} \\ J_{as}^{(1)} & J_{aa}^{(1)} & 0 & \omega_a & J_{as}^{(1)} & J_{aa}^{(1)} \\ J_{ss}^{(2)} & J_{as}^{(2)} & J_{ss}^{(1)} & J_{as}^{(1)} & \omega_s & 0 \\ J_{as}^{(2)} & J_{aa}^{(2)} & J_{as}^{(1)} & J_{aa}^{(1)} & 0 & \omega_a \end{pmatrix} \quad \text{(S4)}$$

Here $\omega_{s/a}$ represents the symmetric/asymmetric NH vibrational frequency and $J_{jk}^{(1)}$ (respectively, $J_{jk}^{(2)}$) represents the inter-strand vibrational coupling between the j-th and k-th vibrational modes in first-neighbor (respectively, second-neighbor) base pairs. In **Table S2** and **Table S3** we summarize the exciton parameters.

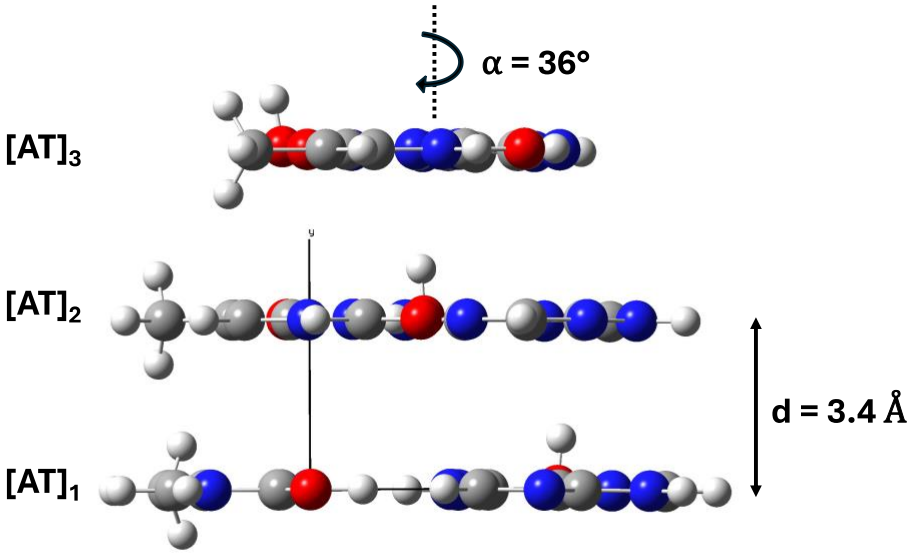

Figure S6. Triple-layer molecular structure of AT base pairs used to parametrize the exciton model.

Coupling constant	Value (cm^{-1})
J^1_{aa}	2.8
J^1_{as}	1.0
J^1_{ss}	2.6
J^2_{aa}	0.4
J^2_{as}	0.3
J^2_{ss}	0.3

Table S3. Computed inter-strand vibrational coupling constants for NH stretching modes for $(dA)_n \cdot (dT)_n$. J^1 represents the coupling between first-neighbor base-pairs whereas J^2 are second-neighbor interactions. a (s) stands for asymmetric (symmetric) NH stretching modes.

Exciton model SFG simulation details

To account for coupling between different AT base pairs in the SFG spectra, we model the $(dA)_{12} \cdot (dT)_{12}$ dsDNA using a coupled exciton Hamiltonian of the form[9, 10]

$$H = \sum_{j=1}^{n} \sum_{m_j} \hbar\omega_{m_j} a^{+}_{m_j} a_{m_j} + \sum_{j=1}^{n} \sum_{k>j}^{n} \sum_{m_j} \sum_{m_k} \hbar J_{m_j m_k} a^{+}_{m_j} a_{m_k} + c.c. \quad \text{(S5)}$$

where n is the total number of base pairs [12 for $(dA)_{12} \cdot (dT)_{12}$], ω_{m_j} represents the m_j-th local mode frequency in the j-th base pair [$m_j = a, s$ in this study], $J_{m_j m_k}$represents the inter-strand vibrational coupling between the m_j-th and m_k-th vibrational modes in the j-th and k-th base pair, and $a^{+}_{m_j}$ and a_{m_j} are creation and annihilation operators of the m_j-th mode. In our model, local mode bases are chosen as the normal modes of a single AT Watson-Crick base pair (see "Exciton model parametrization" section for further details). In **Table S2** and **Table S3** we summarize the exciton parameters.

In **Figure S7** we present the $(dA)_{12} \cdot (dT)_{12}$ dsDNA model used to simulate the SFG spectra in the NH stretching region. The model is consistent with the average values of an ideal B-DNA, with distances and relative orientations between the layers of 3.4 Å and 36°, respectively. The exciton Hamiltonian is constructed for this model and diagonalized to obtain the delocalized exciton energies ω_q and eigenvectors $\bar{u}_q$. The transition dipole and transition polarizability tensor elements of a given exciton normal mode are given by a linear combination of the $2n$ local transition dipole and transition polarizability of the basis modes, namely

$$\mu_{i,q} = \bar{u}_q \cdot \bar{d}_i \tag{S6}$$

$$\alpha_{ij,q} = \bar{u}_q \cdot \bar{\pi}_{ij} \tag{S7}$$

where $\bar{d}_i$ and $\bar{\pi}_{ij}$ $(i,j = x,y,z)$ are vectors containing the transition dipole and transition polarizability elements of the $2n$ localized normal modes. The latter correspond to the values obtained for a single AT Watson-Crick base pair (see **Table S2**) but reoriented so that the reference molecular frame (see **Figure S4**) coincides with the actual orientation of the particular base pair considered in the $(dA)_{12} \cdot (dT)_{12}$ model in **Figure S7**.

Once $\mu_{i,q}$ and $\alpha_{ij,q}$ are computed, the intensity of the q-th exciton SFG peak is determined by the second-order hyperpolarizabilities $\beta^{(2)}_{ijk,q} = \alpha_{ij,q}\mu_{k,q}$. We remark that $\beta^{(2)}_{ijk,q}$ is still given in the fixed molecular frame of the model. To obtain the SFG spectra in the laboratory frame (X,Y,Z), the hyperpolarizability $\beta^{(2)}_{ijk,q}$ is rotated and averaged over the azimuthal angle ϕ in 5° increments, giving rise to the second-order susceptibility $\chi^{(2)}_{IJK,q} = \sum_{ijk}\langle R_{Ii}R_{Jj}R_{Kk}\rangle\, \beta^{(2)}_{ijk,q}$, where R_{Ii} represent elements of the ZYZ Euler rotation matrix.[11] The heterodyne SFG spectrum is computed as

$$Im[\chi^{(2)}] = \mathrm{Im}\sum_q \frac{\chi^{(2)}_{psp,q}}{\omega_{IR} - \omega_q + i\Gamma_q} \tag{S8}$$

with the chiral effective *psp* susceptibilities

$$\chi^{(2)}_{psp,q} = L_{ZYX}\chi^{(2)}_{ZYX,q} - L_{XYZ}\chi^{(2)}_{XYZ,q} \tag{S9}$$

where L_{ijk} are Fresnel factors that depend on the refractive index of the interface as well as the incident angle of the lasers.[12, 13] The Fresnel factors used in this study are listed in **Table S4**. To facilitate comparisons with experiments, exciton frequencies were scaled by 0.95 and Γ_q was set to 4.0 cm^{-1}. This analysis is ambiguous with respect to the experimental definition of phase established in equation (1) of the main text; accordingly, the resulting heterodyne spectra were multiplied by a factor of -1 to capture the phase observed in experiments.

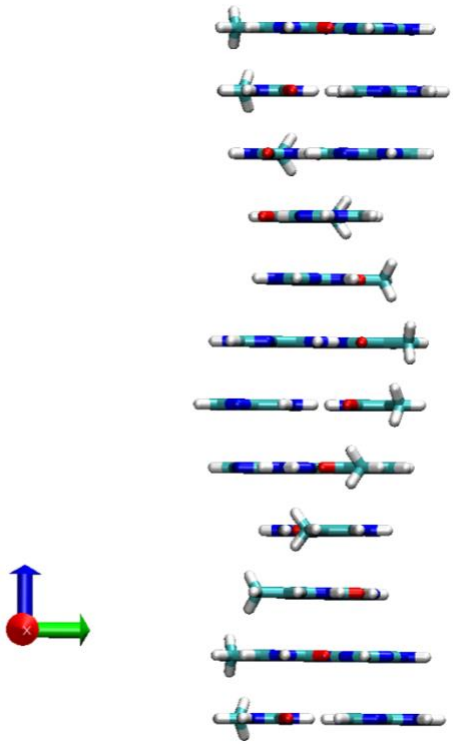

Figure S7. Molecular structure of the $(dA)_{12} \cdot (dT)_{12}$ dsDNA model used to simulate SFG spectra of the NH stretches. The model is consistent with the average values of an ideal B-DNA, with distances and relative orientations between the layers of 3.4 Å and 36°, respectively.

Fresnel Factor	Value
L_{ZYX}	0.140
L_{XYZ}	0.169

Table S4. Fresnel Factors for the *psp* polarization. Fresnel factors determined using a 3-layer model.[12, 13] The refractive index of the interfacial layer is assumed to be 1.465, and the refractive index of air and silica was taken to be 1 and 1.52, respectively. The angle of incidence for the 18800 cm^{-1} visible light (2900 cm^{-1} IR light) is 45° (56°).

Exciton model SFG analysis

In **Figure S8** we present the calculated *psp* SFG spectra obtained from the exciton model for the $(dA)_{12} \cdot (dT)_{12}$ dsDNA in the N-H stretching region for representative orientations of the double strand with respect to the light plane of incidence. The spectra are characterized by two bands centered at $\sim$3205 cm^{-1} and $\sim$3330 cm^{-1}, corresponding to the symmetric and asymmetric NH stretching of the NH_2 group, respectively. Each band is comprised of 12 excitonic vibrations delocalized over the whole double strand, corresponding to different linear combinations of symmetric/asymmetric NH stretching modes on different base pairs. Quite interestingly, the overall signal is a result of a subtle interference between these modes and strongly depends on the overall orientation of the $(dA)_{12} \cdot (dT)_{12}$ dsDNA, characterized by the tilt angle θ of the strand with respect to the surface normal and the twist angle ψ with respect to the symmetry axis of the strand. Note that for certain orientations the high-frequency band is even split into negative and positive peaks (e.g., $\theta = 30°$ and $\psi = 150°$), similar to what is observed experimentally. In **Figure S9** we present the SFG spectra for orientations that reproduce the experimental result. As can be observed, the high-frequency band is characterized by two peaks with opposite phases that correspond to different linear combinations of asymmetric NH stretching modes, whose relative intensity is controlled by the twist angle ψ. Similarly, the symmetric NH low-frequency band also presents two peaks with opposite phases, although the positive peak is suppressed for certain orientations of the double strand. The spectrum corresponding to $\theta = 20°$ and $\psi = 150°$ is the one used in the main text.

For completeness, we also investigate the effect of averaging over the twist angle, corresponding to the assumption that the DNA has cylindrical symmetry. In **Figure S10** we present the results of such analysis. Upon averaging over the axis of symmetry of the strand, the rich interference pattern observed in **Figure S8** and **Figure S9** is lost, giving rise to well-defined low- and high-frequency bands with opposite signs regardless of the orientation of the strand with respect to the light incidence plane.

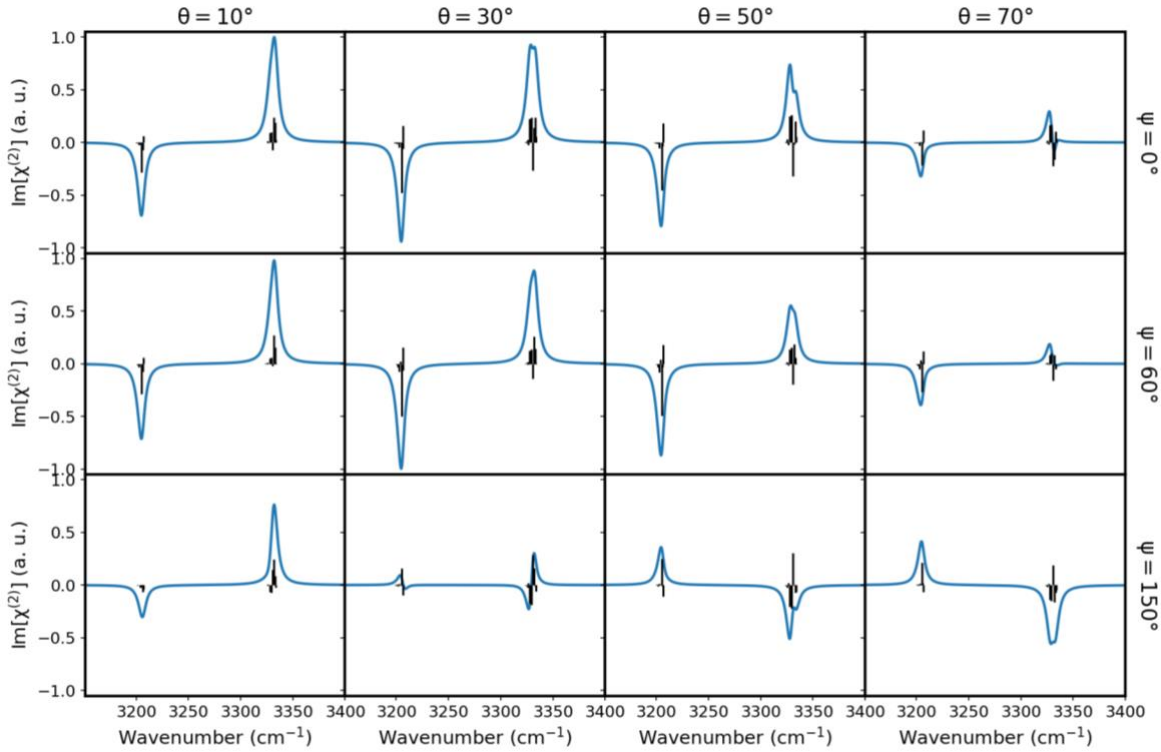

Figure S8. Calculated *psp* SFG spectra in the N-H stretching region for an exciton $(dA)_{12} \cdot (dT)_{12}$ dsDNA model, computed for different tilt and twist orientations of the double-strand with respect to the light plane of incidence. Lines show the vibrational intensity and phase of each excitonic vibrational mode.

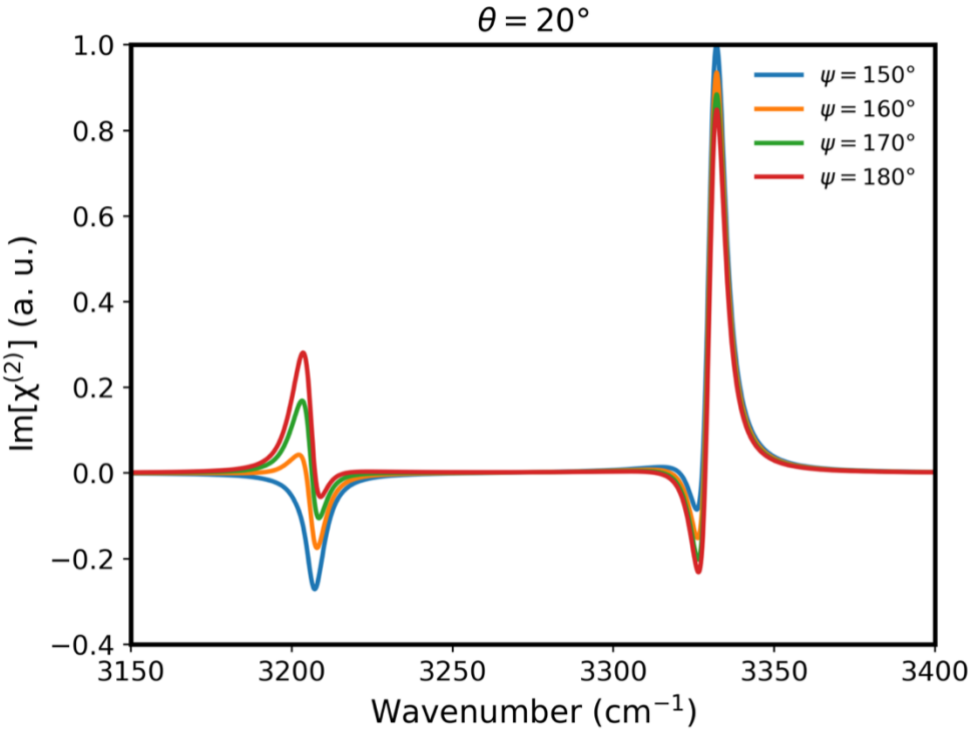

Figure S9. Calculated *psp* SFG spectra in the N-H stretching region in a $(dA)_{12} \cdot (dT)_{12}$ dsDNA model for different orientations of the double strand that closely match the experimental spectra.

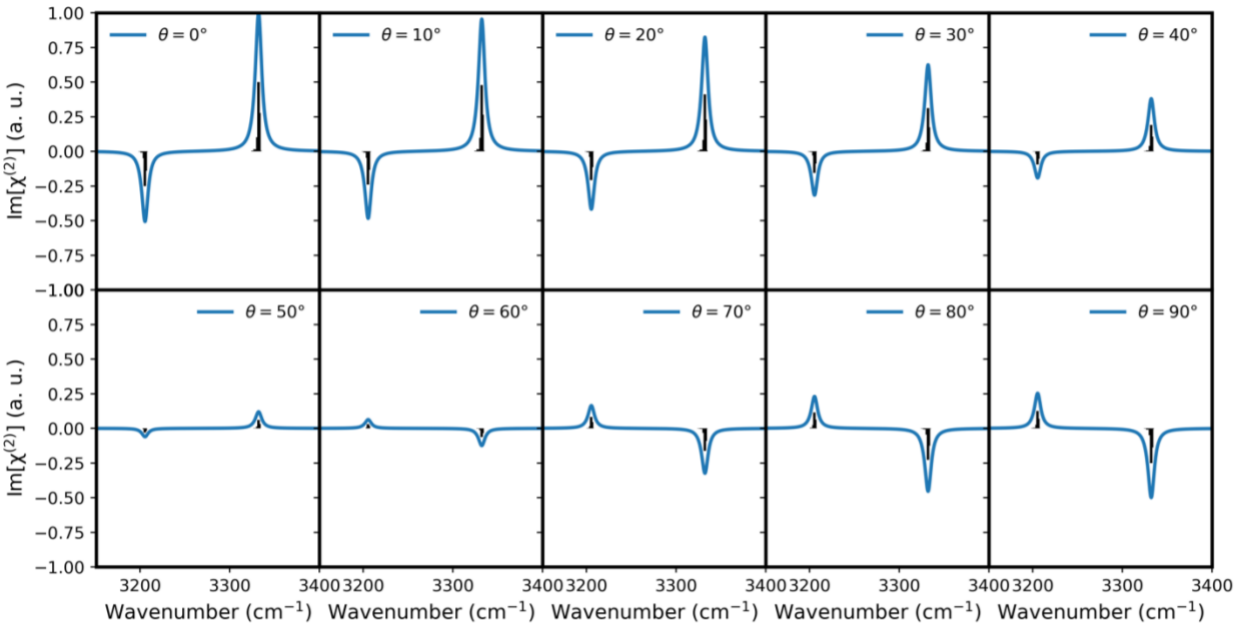

Figure S10. Calculated *psp* SFG spectra in the N-H stretching region for an exciton $(dA)_{12} \cdot (dT)_{12}$ model averaged over the twist angle, computed for different tilt orientations of the double strand with respect to the light plane of incidence. Lines show the vibrational intensity and phase of each excitonic vibrational mode.

References

(1) McDermott, M. L.; Vanselous, H.; Corcelli, S. A.; Petersen, P. B. "DNA's Chiral Spine of Hydration," *ACS Central Science* 3(7), 708-714 (2017). https://doi.org/10.1021/acscentsci.7b00100

(2) Ho, J. J.; Skoff, D. R.; Ghosh, A.; Zanni, M. T. "Structural Characterization of Single-Stranded DNA Monolayers Using Two-Dimensional Sum Frequency Generation Spectroscopy," *J Phys Chem B* 119(33), 10586-10596 (2015). https://doi.org/10.1021/acs.jpcb.5b07078

(3) Peng, C. S.; Jones, K. C.; Tokmakoff, A. "Anharmonic Vibrational Modes of Nucleic Acid Bases Revealed by 2D IR Spectroscopy," *J. Am. Chem. Soc.* 133(39), 15650-15660 (2011). https://doi.org/10.1021/ja205636h

(4) Chai, J.-D.; Head-Gordon, M. "Long-range corrected hybrid density functionals with damped atom–atom dispersion corrections," *Phys. Chem. Chem. Phys.* 10(44), 6615-6620 (2008), 10.1039/B810189B. https://doi.org/10.1039/B810189B

(5) Dunning, T. H., Jr. "Gaussian basis sets for use in correlated molecular calculations. I. The atoms boron through neon and hydrogen," *J. Chem. Phys.* 90(2), 1007-1023 (1989). https://doi.org/10.1063/1.456153

(6) Lee, C.; Park, K.-H.; Cho, M. "Vibrational dynamics of DNA. I. Vibrational basis modes and couplings," *J. Chem. Phys.* 125(11), 114508 (2006). https://doi.org/10.1063/1.2213257

(7) Choi, J.-H.; Cho, M. "Computational IR spectroscopy of water: OH stretch frequencies, transition dipoles, and intermolecular vibrational coupling constants," *J. Chem. Phys.* 138(17), 174108 (2013). https://doi.org/10.1063/1.4802991

(8) Choi, J.-H.; Ham, S.; Cho, M. "Local Amide I Mode Frequencies and Coupling Constants in Polypeptides," *The Journal of Physical Chemistry B* 107(34), 9132-9138 (2003). https://doi.org/10.1021/jp034835i

(9) Hamm, P.; Zanni, M. *Concepts and Methods of 2D Infrared Spectroscopy*; Cambridge University Press, 2011.

(10) Krummel, A. T.; Zanni, M. T. "DNA Vibrational Coupling Revealed with Two-Dimensional Infrared Spectroscopy: Insight into Why Vibrational Spectroscopy Is Sensitive to DNA Structure," *The Journal of Physical Chemistry B* 110(28), 13991-14000 (2006). https://doi.org/10.1021/jp062597w

(11) Yan, E. C.; Fu, L.; Wang, Z.; Liu, W. "Biological macromolecules at interfaces probed by chiral vibrational sum frequency generation spectroscopy," *Chem Rev* 114(17), 8471-8498 (2014). https://doi.org/10.1021/cr4006044

(12) Zhuang, X.; Miranda, P. B.; Kim, D.; Shen, Y. R. "Mapping molecular orientation and conformation at interfaces by surface nonlinear optics," *Physical Review B* 59(19), 12632-12640 (1999). https://doi.org/10.1103/PhysRevB.59.12632

(13) Wang, H. F.; Velarde, L.; Gan, W.; Fu, L. "Quantitative sum-frequency generation vibrational spectroscopy of molecular surfaces and interfaces: lineshape, polarization, and orientation," *Annu Rev Phys Chem* 66189-216 (2015). https://doi.org/10.1146/annurev-physchem-040214-121322